State-dependent climate sensitivity in past warm climates and its implications for future climate projections

Rodrigo Caballero[a] and Matthew Huber[b,1]

[a]Department of Meteorology and Bolin Centre for Climate Research, Stockholm University, 10691 Stockholm, Sweden; and [b]Purdue Climate Change Research Center and Department of Earth, Atmospheric, and Planetary Sciences, Purdue University, West Lafayette, IN 47907

Edited by Kerry A. Emanuel, Massachusetts Institute of Technology, Cambridge, MA, and approved July 10, 2013 (received for review February 22, 2013)

Projections of future climate depend critically on refined estimates of climate sensitivity. Recent progress in temperature proxies dramatically increases the magnitude of warming reconstructed from early Paleogene greenhouse climates and demands a close examination of the forcing and feedback mechanisms that maintained this warmth and the broad dynamic range that these paleoclimate records attest to. Here, we show that several complementary resolutions to these questions are possible in the context of model simulations using modern and early Paleogene configurations. We find that (*i*) changes in boundary conditions representative of slow "Earth system" feedbacks play an important role in maintaining elevated early Paleogene temperatures, (*ii*) radiative forcing by carbon dioxide deviates significantly from pure logarithmic behavior at concentrations relevant for simulation of the early Paleogene, and (*iii*) fast or "Charney" climate sensitivity in this model increases sharply as the climate warms. Thus, increased forcing and increased slow and fast sensitivity can all play a substantial role in maintaining early Paleogene warmth. This poses an equifinality problem: The same climate can be maintained by a different mix of these ingredients; however, at present, the mix cannot be constrained directly from climate proxy data. The implications of strongly state-dependent fast sensitivity reach far beyond the early Paleogene. The study of past warm climates may not narrow uncertainty in future climate projections in coming centuries because fast climate sensitivity may itself be state-dependent, but proxies and models are both consistent with significant increases in fast sensitivity with increasing temperature.

superrotation | hyperthermal

The early Paleogene (~65–35 Mya) was the most recent time when the atmospheric carbon dioxide (CO_2) concentration was in the ≥1,000-ppm range that may reoccur over the next several centuries (1). Study of this period may therefore provide constraints on climate sensitivity, broadly defined as the global mean temperature response to radiative forcing, which are useful for climate change prediction (2, 3). On the other hand, analogies between early Paleogene and future climates are not straightforward because so many other variables apart from CO_2 have also changed (4), and because climate sensitivity may change across different climate states (3, 5). Given the crucial role that paleoclimate data from past greenhouse climates play in informing the debates about future climate change (6, 7), an investigation of the strengths and limitations of using such data to make inferences about climate sensitivity is in order.

Recent progress in reconstructing the early Paleogene has brought an across-the-board upward revision of surface temperature estimates. Tropical sea surface temperatures (SSTs), previously thought to be similar to or even cooler than modern SSTs, were 3–10 °C warmer than today (8–12), although uncertainty on these values remains large (13). Extratropical surface temperatures were 10–40 °C warmer than modern extratropical surface temperatures in continental interiors (14–18), along polar margins (19, 20), and over the oceans (21). Here, we compile these proxy interpretations to estimate that the global area-weighted annual mean surface temperature (MAT) in the early Eocene, the warmest part of the early Paleogene, was some 13 ± 2.6 °C warmer than modern temperatures (Fig. 1; uncertainty is 2 SEs, as described in *Methods*) and not ~4 °C warmer, as previously thought (22). This tripling in estimated warming calls for a reassessment of the forcing and feedback mechanisms that sustained such elevated temperatures.

On the forcing side, atmospheric partial pressure of CO_2 (pCO_2) in the early Paleogene is reconstructed to have been higher than modern, although the range of reconstructed values is large (23–28). It is also possible that methane concentrations were higher than modern concentrations (29), although the lack of direct methane proxies means that only indirect model-based estimates are available (30).

On the feedback side, it is necessary to distinguish between "fast" feedbacks, associated with changes in water vapor, lapse rate, clouds, snow cover, and sea ice, and slower "Earth system" feedbacks, including changes in ice sheets and vegetation cover as well as modifications in atmospheric composition resulting from altered biogeochemical cycles.

Discussions of future climate change generally revolve around fast climate sensitivity, defined as the equilibrium change of surface temperature in response to radiative forcing equivalent to a doubling of pCO_2 ($\Delta T_{2\times}$) when only fast feedbacks are allowed to act (31). The value of $\Delta T_{2\times}$ is highly uncertain (32); it varies from model to model, is sensitive to model parameters, and is not well constrained by observations. Estimates for modern conditions range from 2.1 to 7.1 °C within the 90% confidence interval (33); this large uncertainty motivates interest in using paleoclimates to help constrain $\Delta T_{2\times}$ (3). On paleoclimate time scales, slow feedbacks have time to act; their overall effect is generally thought to be positive, so that the resulting Earth system sensitivity (ESS) is thought to be greater than $\Delta T_{2\times}$ (3, 34, 35).

The Paleocene–Eocene Thermal Maximum and other hyperthermal events (36–38) are often discussed as analogs for anthropogenic climate change because they involve carbon cycle and climate perturbations that are rapid by geological standards (6). That these large warmings occurred in an already warm background climate imply either that strong positive Earth system feedbacks operated on 1- to 100-kyr (thousand-year) time scales or that fast sensitivity was very strong (or, of course, some combination of both) (2, 7). It is often implicitly assumed that

Author contributions: R.C. and M.H. designed research, performed research, and wrote the paper.

The authors declare no conflict of interest.

This article is a PNAS Direct Submission.

Freely available online through the PNAS open access option.

[1]To whom correspondence should be addressed. E-mail: huberm@purdue.edu.

This article contains supporting information online at www.pnas.org/lookup/suppl/doi:10.1073/pnas.1303365110/-/DCSupplemental.

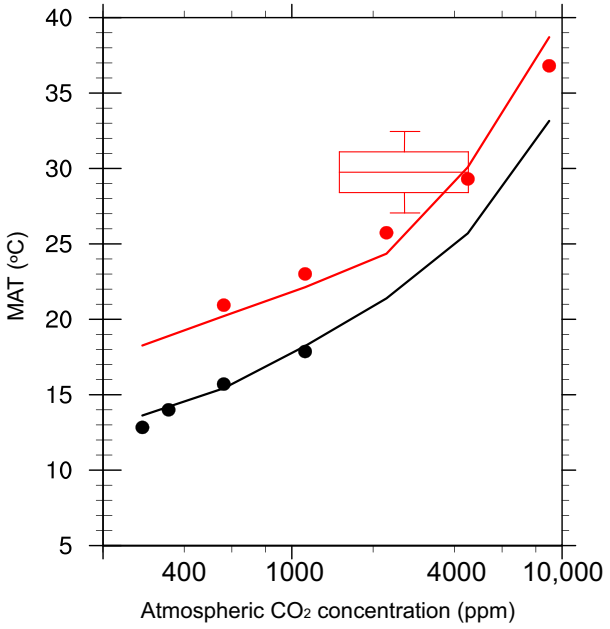

Fig. 1. Global mean surface temperature and MAT in simulations with modern (black) and Paleogene (red) boundary conditions. Dots show results from fully coupled simulations, and lines show results from slab-ocean simulations. The red box-and-whisker plot shows a proxy data-based estimate for the early Eocene (*Methods*). The vertical limits on the box and whisker are 1 and 2 SEs on the mean MAT value, respectively. The horizontal extent of the box spans a range of CO_2 values encompassing our best guess of the likely range of values based on the references cited in the main text.

the inferred strong positive feedbacks can be generalized and that they apply to the future (2). An alternative perspective is that fast feedbacks may be strongly state-dependent, in which case even perfect knowledge of a past fast sensitivity may not provide an accurate guide to its modern value.

Here, we study the mechanisms responsible for maintaining an elevated early Paleogene temperature using a suite of modern and early Paleogene climate model simulations spanning a broad range of radiative forcing, controlled by atmospheric CO_2 concentrations ranging over five successive doublings from 280 to 8,960 ppm (*Methods*). Comparison between the early Paleogene and modern runs permits evaluation of Earth system feedbacks associated with changed ice sheets and vegetation cover. We also quantify the changes in fast climate sensitivity and associated feedbacks across the early Paleogene simulations.

Until recently, attempts to simulate the early Paleogene using conventional climate models failed to match the weak equator-to-pole surface temperature gradients and warm winter continental interiors implied by earlier proxy temperature reconstructions (e.g., ref. 39). This raised fundamental questions about our ability to model these climates (7, 40). An important consequence of the progress in reconstructing early Paleogene temperatures is that it greatly ameliorates this model-data mismatch because models are better able to reproduce warmer poles and reduced temperature gradients when tropical SSTs are allowed to warm above modern SSTs (41). For example, comparison of simulations conducted by five different modeling groups against newer early Eocene proxy data [the informal Eocene Model Intercomparison Project (EoMIP)] found that most models can broadly match this newer data, including weaker meridional gradients, given sufficiently large greenhouse gas forcing (42). Among the models included in the EoMIP, the Community Climate System Model version 3 (CCSM3) of the National Center for Atmospheric Research (NCAR) (the model used in the present paper; *Methods*) gave the closest match to data, likely because the CCSM3's vigorous polar amplification (43) allows it to match high-latitude temperature records well once the global mean value is warm enough. Although significant discrepancies with individual data points remain (14, 21), this match represents a very considerable improvement compared with earlier modeling work, adding credibility to model-based studies of early Paleogene sensitivity.

Results

Fig. 1 shows the global and annual mean temperature for all simulations as a function of atmospheric CO_2. Note that the early Paleogene simulation at 4,480 ppm of CO_2 produces a global mean temperature very close to the early Eocene proxy data estimate (14). Two main features are immediately apparent from this figure. First, there is a ~5 °C offset between global mean temperature in the early Paleogene and in modern cases that is roughly constant across all levels of forcing. This demonstrates that a large fraction of the temperature difference between modern and early Paleogene conditions is not directly attributable to CO_2 radiative forcing. Second, in both early Paleogene and modern simulations, the temperature gain with each doubling of CO_2 is not constant but increases with increasing CO_2. This implies either radiative forcing that is not logarithmic in CO_2 concentration and/or a fast climate sensitivity that is not constant as climate changes. As it turns out, both are true in this model. We discuss each of these issues in turn below.

ESS. The offset between modern and early Paleogene simulations shows that the changes in boundary conditions, including removal of ice sheets and replacement with vegetation, movement of continents, changes in ocean currents, and changes in aerosols, have large impacts on global mean temperature. Some of these factors, such as changes in ice sheet distribution, might reasonably be called Earth system feedbacks because they are internally determined as part of the climate system. Other factors, such as continental position or ocean gateway changes, are nonradiative external forcings that do not arise as part of climate feedback.

Detailed analysis of the factors that sum to produce the modeled temperature offset of 5 °C finds that it is largely due to surface albedo differences (42). These arise not only in high latitudes, as a direct consequence of the specified changes in terrestrial ice, but in low latitudes. Study of the high-latitude temperature change due to changing specified land ice (44) shows that the induced change is likely <1 °C, so that component is only a small fraction of the 5 °C offset. The decrease in tropical-to-subtropical albedo, which causes most of the temperature change, is due to increased early Paleogene vegetation cover in present-day deserts (42). In a model with truly interactive ice and vegetation, these would rightfully be included within the definition of ESS to CO_2.

A fraction of the offset can also be ascribed to changes in aerosol forcing. In our early Paleogene simulations, direct aerosol forcing is greatly reduced by choice from modern conditions (indirect effects are not explicitly included in the model). Comparison between the results of simulations using identical models and nearly identical boundary conditions but different treatments of aerosols (42) suggests that almost 2 °C of this offset can be explained by aerosol choices, which are necessarily poorly constrained. Very little of the net temperature change between modern and early Paleogene conditions is explained by paleogeography or rectification between changes in meridional heat transports and global mean temperatures (42).

These results are likely to be sensitive both to assumptions about vegetation that are poorly constrained by data and to model cloud feedbacks that are likely to be strongly model-dependent. We can conclude, however, that in this model at least,

large changes can be introduced by processes that may reasonably be called Earth system feedbacks and that data-based estimates of early Paleogene ESS (from paleoclimate proxy records of temperature and estimates of pCO_2) may yield values substantially enhanced above that of fast sensitivity, as previously proposed (3). Changes in aerosol forcing remain a large source of uncertainty, and future work is necessary in this key area (45).

Increasing Efficacy of CO_2 Forcing. To understand better the reasons for the nonconstant response to successive doublings of CO_2 seen in Fig. 1, we apply standard methods for the quantification of climate forcing, sensitivity, and feedback strengths in the early Paleogene simulations. Specifically, we use the method of Gregory et al. (46) to separate forcing and sensitivity, and the "partial radiative perturbation" (PRP) method (47) to estimate the strengths of the various fast feedbacks (*Methods*). The PRP method provides an independent estimate of the overall climate sensitivity, and intercomparison with the estimates of Gregory et al. (46) gives a measure of the robustness of our results. We expect some difference between the two estimates because the PRP method assumes that all feedback mechanisms are linearly independent, whereas the Gregory method includes the effects of nonlinear interaction among different mechanisms.

The radiative forcing caused by each doubling of pCO_2 (Fig. 2*A*) increases with increasing pCO_2 and temperature: In the coldest simulations, the forcing is ∼3.5 $W{\cdot}m^{-2}$ per doubling, a number familiar from sensitivity studies under modern conditions, but it roughly doubles to ∼7 $W{\cdot}m^{-2}$ per doubling in the warmest runs. Part of the enhanced temperature response to CO_2 doubling found at the upper range of temperatures (Fig. 1) must therefore be attributed to increasing efficacy of CO_2 radiative forcing. This increasing efficacy of CO_2 in climate model simulations has been noted before (48, 49), but its underlying causes have not been identified previously. Possibilities include nonlogarithmic behavior of CO_2 opacity at high concentrations (50); changes in the background temperature, water vapor, and cloud distributions with rising surface temperature that enhance forcing by CO_2; and increasing "ultrafast" cloud adjustment, that is, cloud responses to instantaneous CO_2 doubling that occur before surface temperature has time to change and can act as an additional source of radiative forcing (51).

Here, we quantify the role of each of these mechanisms. Radiative forcing due to ultrafast cloud adjustment (Fig. 2*A*; details are provided in *Methods*) is near zero in the coldest run but grows to around 1.8 $W{\cdot}m^{-2}$ in the warmest run, accounting for half of the overall increase of ∼3.5 $W{\cdot}m^{-2}$ in forcing across the simulations. To determine the origin of the remaining half, we use an offline radiation code and climatological temperature, humidity, and cloud fields taken from the general circulation model (GCM) simulations to estimate the change in CO_2 forcing when each of these fields, as well as background CO_2, is varied independently (details are provided in *Methods*). The results (Fig. 2*B*) point to nonlogarithmic CO_2 opacity as the main culprit. Changing temperature structure provides a modest increase in the efficacy of CO_2 forcing, which is almost exactly cancelled by a drop in efficacy due to increased masking by humidity and clouds.

State-Dependent Specific Climate Sensitivity. It is clear from Fig. 3*A* that specific climate sensitivity, the temperature response per unit of radiative forcing, also increases sharply at higher temperatures in this model. The sensitivity estimates provided by the method of Gregory et al. (46) and PRP method differ somewhat at the low end, but both give values in the range of 0.6–0.8 $W{\cdot}m^{-2}{\cdot}K^{-1}$, consistent with studies of modern climate sensitivity. Above a global mean temperature of ∼23 °C, however, the estimates of both Gregory et al. (46) and PRP rise sharply to a value roughly twice as high. To understand the proximate causes for this large increase in sensitivity, Fig. 2*C* presents PRP estimates of the contribution made by each fast feedback mechanism. Surface albedo feedback makes an essentially negligible contribution throughout, because there is little snow and sea ice in these relatively warm climates. Water vapor feedback makes an increasing contribution with temperature, which is offset by an increasingly negative lapse rate feedback, so that their sum is roughly constant with temperature, albeit with some increase at the highest temperatures. The Planck feedback is also roughly constant at about −3.5 $W{\cdot}m^{-2}{\cdot}K^{-1}$ in all simulations.

This leaves cloud feedback as the main driver of increased high-temperature–specific sensitivity. Short-wave cloud feedback increases sharply from about −0.5 to +0.5 $W{\cdot}m^{-2}{\cdot}K^{-1}$ as global MAT crosses the 23 °C threshold and increases a further 0.5 $W{\cdot}m^{-2}{\cdot}K^{-1}$ as MAT approaches 30 °C. Long-wave cloud feedback exhibits a partly offsetting downward trend; nonetheless,

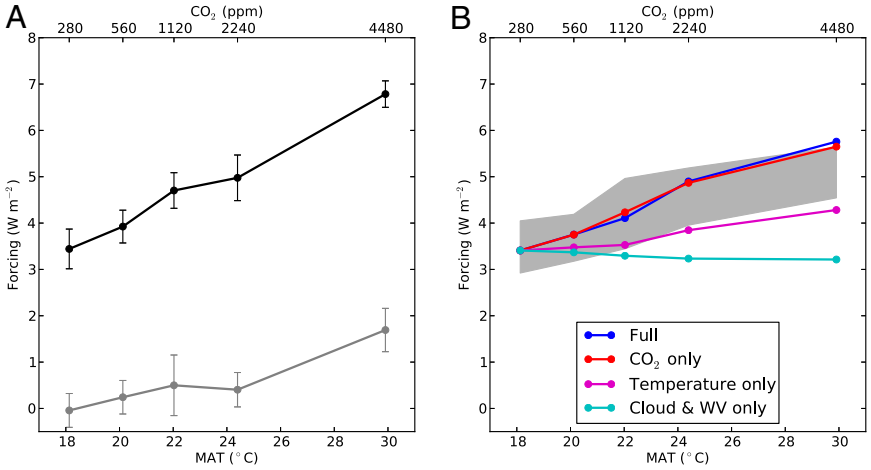

Fig. 2. Forcing analysis for the early Paleogene simulations. (*A*) Radiative forcing due to a doubling of CO_2 as a function of global mean surface temperature and MAT (black line) and contribution to the forcing due to ultrafast cloud adjustment (gray line). Error bars represent 95% confidence intervals. (*B*) Offline radiative forcing calculations using simulated climatological temperature, humidity, and cloud fields (*Methods*). Lines show results when all fields, as well as baseline CO_2, vary (blue); when only baseline CO_2 varies (red); when only temperature varies (magenta); and when only humidity and clouds vary (cyan). Gray shading shows total forcing minus the ultrafast cloud adjustment component (i.e., the difference between the black and gray lines in *A*). WV, water vapor.

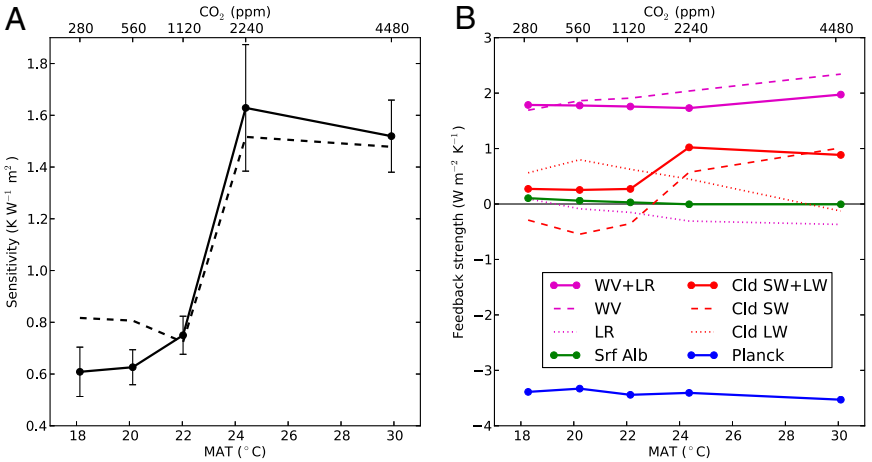

Fig. 3. Feedback analysis for the early Paleogene simulations. (*A*) Specific climate sensitivity as a function of global mean surface temperature and MAT computed using the method of Gregory et al. (46) (solid line) and the PRP method (dashed line). Error bars represent 95% confidence intervals. (*B*) Strengths of individual feedback mechanisms as a function of global mean surface temperature and MAT: surface albedo (Alb) feedback (green line); WV feedback (dashed magenta line), lapse rate feedback (dotted magenta line), and their sum (solid magenta line); cloud short-wave (SW) feedback (dashed red line); cloud long-wave (LW) feedback (dotted red line); total cloud feedback (solid red line); and Planck feedback (blue line).

the overall cloud feedback shows a sharp rise at temperatures above 23 °C. This transition corresponds to the passage from the three-doublings (2,240 ppm of CO_2) to the four-doublings (4,480 ppm of CO_2) case. Examination of the total cloud cover for these two cases (Fig. S1) shows a sharp drop in tropical cloud cover in the warmer case, combined with significant change in the southern extratropics. This drop in cloud cover is a positive feedback because it leads to decreased cooling due to diminished short-wave cloud forcing, especially in the tropical Pacific and the Southern Hemisphere midlatitudes (Fig. S1).

Discussion and Implications

We have analyzed a suite of climate model simulations spanning a broad range of greenhouse gas forcing under both modern and early Paleogene conditions. Our key findings are fourfold.

First, recently revised proxy temperature reconstructions for the early Paleogene indicate much warmer conditions than previously thought. As described in *Methods*, the proxy data compilation reveals global mean temperatures ∼13 °C warmer than present global mean temperatures. This is a roughly threefold increase over previous proxy estimates of ∼4 °C warming (22). This estimate is independently confirmed by analyzing the global mean temperatures produced by climate model simulations that are the best fit to proxies on a point-by-point basis (14, 42) Such extreme warming compared with current temperatures requires some combination of very strong radiative forcing in the early Paleogene compared with modern conditions and/or enhanced climate sensitivity due to strong positive feedbacks of either the fast or slow variety.

Second, early Paleogene simulations are uniformly warmer than modern simulations at the same CO_2 by ∼5 °C, mainly due to changes in low-latitude surface albedo and direct aerosol effects. This temperature offset quantifies the effect of at least some of the relevant slow Earth system feedbacks helping to maintain elevated early Paleogene temperatures. It is entirely possible, however, that other slow feedbacks not included in these simulations may also play an important role. For example, indirect aerosol effects could have important consequences for cloud climatology, resulting in radiative forcing potentially comparable to that due to several doublings of CO_2 (45).

Third, the radiative forcing due to a doubling of CO_2 increases by about a factor of 2 from across the simulations, due in roughly equal parts to increased forcing by ultrafast cloud adjustment and nonlogarithmic behavior of CO_2 opacity. Both of these effects are small for small perturbations around modern climates, and little attention has been paid to their evolution at high CO_2. The important role they play in maintaining warm Paleogene climates in this model motivates more detailed study in a range of different models.

Finally, fast-feedback sensitivity in the present model is strongly nonuniform, increasing rapidly at high temperatures due mostly to positive short-wave cloud feedbacks. These changes in cloud cover and cloud radiative forcing (CRF) are coincident with major changes in the model's general circulation. As shown in previous work (52), the 23 °C threshold marks the transition to a regime in which large-amplitude equatorial waves reminiscent of the Madden–Julian oscillation converge sufficient zonal momentum onto the equator to drive mean superrotating (i.e., westerly) winds along the equatorial upper troposphere. This transition is also observed in a "superparameterized" version of the atmosphere model (53), where the standard convective parameterization is replaced by an embedded cloud-resolving model within each column that is arguably closer to physical reality. The transition coincides with a substantial weakening of the Hadley cell, which is consistent with decreased high- and midlevel cloud cover in the deep tropics and with low-level clouds in the subtropics (Fig. S2). Moreover, as temperature increases, the midlatitude storm tracks become weaker and shift poleward, resulting in decreased low and midlevel clouds, especially in the southern midlatitudes (Fig. S2). There is observational support for the notion that such a shift in storm tracks is associated with positive cloud feedback (54).

Considerable further work is required to unravel fully the radiative–dynamic interactions that underpin the state-dependent sensitivity documented here. To be sure, our results are from a single model and rely heavily on cloud feedbacks, probably the worst-constrained component of current climate models, so they are almost certain to change substantially in other models. Indeed, a study using the Australian Bureau of Meteorology Research Centre model found no evidence for increased fast sensitivity even at very high CO_2 (49).

We do not claim that our findings necessarily reflect true attributes of the real climate system. Nevertheless, our results reveal that it is physically plausible that slow feedbacks played a major role in maintaining warm conditions during the early Paleogene, and that the strength of fast feedbacks may depend

strongly on the background climate state. Given the uncertainty in current understanding of cloud feedbacks, it is possible that such fast sensitivity transitions could occur under cooler conditions (e.g., the Pliocene, the future) than we have simulated here.

Although the importance of slow feedbacks has been proposed before, few studies have demonstrated their existence or recognized that strong interactions can occur between these slow feedbacks and state-dependent fast sensitivity as shown here. Only fast climate feedbacks are relevant for climate change in the near future, but when dealing with paleoclimates, we must contend with the fact that slow and fast feedbacks act together. That we do not even have a complete catalog, much less a quantification, of all relevant slow feedbacks means that attempts to constrain fast climate sensitivity from paleoproxy data are subject to large and currently unquantifiable uncertainty. Further, the possibility of state-dependent fast climate sensitivity highlighted here implies that even if an interval, such as a hyperthermal, can be found for which it is reasonable to exclude an important role for slow feedbacks, it is not obvious that the resulting value of fast climate sensitivity has relevance for the modern world. At bottom, this is a problem of equifinality (55, 56): Different combinations of forcing and feedbacks (both fast and slow) can maintain observationally indistinguishable climates, and we are currently unable to constrain independently the particular mix of contributions that prevails in the real system.

Given the current state of knowledge, attempts to estimate near-future climate sensitivity directly from deep-time proxy data must be handled with caution. Breaking the equifinality deadlock requires a quantitative disentangling of the various contributions to warming; this necessarily involves the use of models, with their attendant uncertainties, and careful consideration of the physical mechanisms involved to establish their plausibility and robustness. Perhaps the most valuable use of paleoclimate proxy data in the context of climate prediction is in model falsification (i.e., in singling out models that more accurately represent climate's dynamic range) (5, 57). These more accurate models may have more predictive power for the future. We can conclude, however, that models and proxies are both compatible with increasing fast sensitivity in warm climates.

Methods

Data-Based Estimate of Early Eocene Global Mean Temperature. The estimate is based on the early Eocene proxy temperature data compilations presented by Huber and Caballero (14) and Hollis et al. (21). The anomalies of individual proxy temperature data points with respect to modern values at the corresponding paleolocation were first calculated. An area-weighted average of these anomalies was then computed; finally, the area-weighted mean anomaly was added to modern global mean surface temperature. The area weighting was carried out by binning the data into three regions (30°N to 30°S, 30°N/S to 60°N/S, and 60°N/S to 90°N/S), computing unweighted averages within the bins and then area-weighted averaging the three bins together to create a global area-weighted mean temperature anomaly. Errors were propagated by combining two types of error. First, a conservative ±5 °C random error on each proxy estimate was assumed. Second, an estimate of the random error introduced by sparse sampling in the spatial domain was included based on the spatial SD over samples within the three regions over which area weighting was carried out. These two sources of error were combined and normalized by the square root of the number of proxy observations, all of which were considered to be independent.

Model and Simulations. We use the NCAR CCSM3 (58, 59). We present results from two sets of simulations using the model in the fully coupled ocean-atmosphere-sea ice-land surface mode at T31 × 3′ resolution (~3.8° and 3 × 1.8° grid spacing in the atmosphere and ocean, respectively). One set of simulations used fixed boundary conditions (topography, vegetation, and bathymetry) developed to simulate the early Paleogene (60). The other set of simulations are standard control runs performed using modern boundary conditions (59). The simulations within each set were identical in all respects except for the atmospheric CO_2 concentration, which took the values of 280, 380, 560, and 1,120 ppm in the modern simulations and 560, 1,120, 2,240, and 4,480–8,960 ppm in the Paleogene simulations. All of these nine simulations were run in fully coupled mode without ocean acceleration until they reached a statistically steady state. In the Paleogene simulations, the solar constant was set at 1,365 $W \cdot m^{-2}$ and a very low aerosol radiative forcing was assumed, as discussed by Lunt et al. (42). The modern runs used a solar constant of 1,367 $W \cdot m^{-2}$ and prescribed modern aerosols. In previous work, we have compared some of the Paleogene simulations with paleoclimate proxies, finding a reasonable level of agreement for major climate events of the early Paleogene, including the Eocene-Oligocene transition (61) and the Early Eocene Climatic Optimum (14, 21, 42). Significant regional data model discrepancies remain, however (14, 21, 42).

For the climate sensitivity, forcing, and feedback analysis, we follow common practice in using the "slab ocean" version of the CCSM3, in which the full dynamic ocean is replaced by a fixed thermodynamic slab with depth and ocean heat convergence prescribed from the fully coupled simulations. The atmospheric model resolution in these simulations was T42 (roughly 2.8° grid spacing), but these simulations were otherwise identical to the fully coupled runs and produced global mean surface temperatures very close to those of coupled runs at the same CO_2 (Fig. 1).

Forcing and Feedback Analysis. To quantify forcing and fast climate sensitivity of the Paleogene runs, we use the method proposed by Gregory et al. (46) involving a linear regression between global mean top-of-atmosphere radiative imbalance and surface temperature anomaly in a slab-ocean model simulation subjected to a stepwise increase in radiative forcing. The regression line's intercept on the radiative imbalance axis estimates the adjusted forcing, whereas its slope gives the fast climate sensitivity. We use a quadrupling of CO_2 as radiative forcing and annual means for the first 20 simulation years to compute the regression (except in the warmest case, in which the simulation becomes numerically unstable after 8 y). Error bars in Figs. 2 and 3 are 95% confidence intervals for the slope and intercept of the regressions.

To estimate the radiative impact of ultrafast cloud adjustment, we follow Andrews et al. (51) and use a similar regression method but applied to CRF output from the simulations; the *y* intercept estimates the radiative forcing due to cloud changes in the early stages of the simulation, when surface temperature has not yet changed. A correction is necessary because CRF will change when CO_2 is doubled even with no change in clouds; this correction is computed using an offline radiation code (see below) applied to the climatological seasonally varying temperature, humidity, and cloud fields from each simulation.

To study CO_2 forcing in the absence of ultrafast cloud adjustment, we compute the top-of-atmosphere radiative perturbation due to instantaneous CO_2 doubling using an offline radiation code applied to climatological temperature, humidity, and cloud fields taken from the GCM simulations. Stratospheric adjustment is accounted for by patching the stratospheric temperature field from the doubled-CO_2 simulation with the tropospheric temperature from the corresponding base simulation. In the first sequence of computations, we use the full set of fields from each of the simulations in turn and the corresponding CO_2 as the base value for the doubling calculation; as expected, the results (blue line in Fig. 2*B*) match the forcing estimated by the method of Gregory et al. (46) well once the effect of ultrafast cloud adjustment is removed (gray shading in Fig. 2*B*). Next, we hold temperature, humidity, and cloud fields fixed at their values from the 280-ppm simulation and allow only the base CO_2 to vary; this quantifies the effect of deviation from logarithmic behavior of CO_2 opacity. The effect of changing temperature structure is quantified by a sequence of computations in which only temperature is varied, holding humidity and cloud distributions fixed at their values from the 280-ppm simulation and base CO_2-fixed at 280 ppm. Finally, the effect of changing water vapor and clouds is determined by an analogous sequence in which cloud and humidity vary but temperature is fixed.

For the feedback analysis, we use the PRP method, which uses an offline radiative transfer calculation to diagnose the top-of-atmosphere radiative perturbation due to changes in temperature, clouds, water vapor, and surface albedo separately. We implement the method following the method of Colman et al. (47), using the radiation code taken from the atmospheric component of the CCSM3 and embedded in the Climate Modeling and Diagnostic Toolkit (CliMT; available from http://people.su.se/~rcaba/climt). The PRP results presented here can be reproduced using the script Cam3-Feedbacks.py distributed with CliMT. The calculations used 5 y of model outputs generated every 6 h.

ACKNOWLEDGMENTS. Some of the simulations presented here were performed on resources provided by the Swedish National Infrastructure for Computing at the National Centre for Supercomputing (Linköping, Sweden).

The fully coupled simulations were carried out at Purdue University at the Rosen Center for Advanced Computing. This is Purdue Climate Change Research Center (PCCRC) publication no. 1303. M.H. was supported by National Science Foundation P2C2 Grant OCE 0902882.

1. Archer D, et al. (2009) Atmospheric lifetime of fossil fuel carbon dioxide. *Annu Rev Earth Planet Sci* 37:117–134.
2. Pagani M, Caldeira K, Archer D, Zachos JC (2006) Atmosphere. An ancient carbon mystery. *Science* 314(5805):1556–1557.
3. PALAEOSENS Project Members (2012) Making sense of palaeoclimate sensitivity. *Nature* 491(7426):683–691.
4. Haywood AM, et al. (2011) Are there pre-Quaternary geological analogues for a future greenhouse warming? *Philos Trans A Math Phys Eng Sci* 369(1938):933–956.
5. Huber M (2013) A sensitivity to history. *Nat Geosci* 6:15–16.
6. Jansen E, et al. (2007) Palaeoclimate. *Climate Change 2007: The Physical Science Basis*, eds Solomon S, et al. (Cambridge Univ Press, Cambridge, UK).
7. Zachos JC, Dickens GR, Zeebe RE (2008) An early Cenozoic perspective on greenhouse warming and carbon-cycle dynamics. *Nature* 451(7176):279–283.
8. Pearson PN, et al. (2001) Warm tropical sea surface temperatures in the Late Cretaceous and Eocene epochs. *Nature* 413(6855):481–487.
9. Pearson PN, et al. (2007) Stable warm tropical climate through the Eocene Epoch. *Geology* 35(3):211–214.
10. Zachos JC, et al. (2003) A transient rise in tropical sea surface temperature during the Paleocene-Eocene thermal maximum. *Science* 302(5650):1551–1554.
11. Head JJ, et al. (2009) Giant boid snake from the Palaeocene neotropics reveals hotter past equatorial temperatures. *Nature* 457(7230):715–717.
12. Jaramillo C, et al. (2010) Effects of rapid global warming at the Paleocene-Eocene boundary on neotropical vegetation. *Science* 330(6006):957–961.
13. Huber M (2008) Climate change. A hotter greenhouse? *Science* 321(5887):353–354.
14. Huber M, Caballero R (2011) The early Eocene equable climate problem revisited. *Climate of the Past* 7:603–633.
15. Greenwood DR, Wing SL (1995) Eocene continental climates and latitudinal temperature gradients. *Geology* 23(11):1044–1048.
16. Kowalski EA, Dilcher DL (2003) Warmer paleotemperatures for terrestrial ecosystems. *Proc Natl Acad Sci USA* 100(1):167–170.
17. Peppe DJ, et al. (2011) Sensitivity of leaf size and shape to climate: Global patterns and paleoclimatic applications. *New Phytol* 190(3):724–739.
18. Snell KE, et al. (2013) Hot summers in the Bighorn Basin during the early Paleogene. *Geology* 41(1):55–58.
19. Eberle JJ, Greenwood DR (2012) Life at the top of the greenhouse Eocene world—A review of the Eocene flora and vertebrate fauna from Canada's High Arctic. *Geol Soc Am Bull* 124(1-2):3–23.
20. Pross J, et al.; Integrated Ocean Drilling Program Expedition 318 Scientists (2012) Persistent near-tropical warmth on the Antarctic continent during the early Eocene epoch. *Nature* 488(7409):73–77.
21. Hollis CJ, et al. (2012) Early Paleogene temperature history of the Southwest Pacific Ocean: Reconciling proxies and models. *Earth Planet Sci Lett* 349-350:53–66.
22. Covey C, Sloan LC, Hoffert MI (1996) Paleoclimate data constraints on climate sensitivity: The paleocalibration method. *Clim Change* 32:165–184.
23. Pearson PN, Palmer MR (2000) Atmospheric carbon dioxide concentrations over the past 60 million years. *Nature* 406(6797):695–699.
24. Lowenstein TK, Demicco RV (2006) Elevated Eocene atmospheric CO_2 and its subsequent decline. *Science* 313(5795):1928.
25. Royer DL, Berner RA, Park J (2007) Climate sensitivity constrained by CO_2 concentrations over the past 420 million years. *Nature* 446(7135):530–532.
26. Beerling DJ, Royer DL (2011) Convergent Cenozoic CO_2 history. *Nat Geosci* 4:418–420.
27. Pagani M, et al. (2011) The role of carbon dioxide during the onset of Antarctic glaciation. *Science* 334(6060):1261–1264.
28. Pearson PN, Foster GL, Wade BS (2009) Atmospheric carbon dioxide through the Eocene-Oligocene climate transition. *Nature* 461(7267):1110–1113.
29. Sloan LC, Walker JC, Moore TC, Jr., Rea DK, Zachos JC (1992) Possible methane-induced polar warming in the early Eocene. *Nature* 357(6376):320–322.
30. Beerling DJ, Fox A, Stevenson DS, Valdes PJ (2011) Enhanced chemistry-climate feedbacks in past greenhouse worlds. *Proc Natl Acad Sci USA* 108(24):9770–9775.
31. Knutti R, Hegerl GC (2008) The equilibrium sensitivity of the Earth's temperature to radiation changes. *Nat Geosci* 1:735–743.
32. Roe GH, Baker MB (2007) Why is climate sensitivity so unpredictable? *Science* 318(5850):629–632.
33. Meinshausen M, et al. (2009) Greenhouse-gas emission targets for limiting global warming to 2 degrees C. *Nature* 458(7242):1158–1162.
34. Lunt DJ, et al. (2010) Earth system sensitivity inferred from Pliocene modelling and data. *Nat Geosci* 3:60–64.
35. Pagani M, Liu Z, LaRiviere J, Ravelo AC (2010) High Earth-system climate sensitivity determined from Pliocene carbon dioxide concentrations. *Nat Geosci* 3:27–30.
36. Lourens LJ, et al. (2005) Astronomical pacing of late Palaeocene to early Eocene global warming events. *Nature* 435(7045):1083–1087.
37. Nicolo MJ, Dickens GR, Hollis CJ, Zachos J (2007) Multiple early Eocene hyperthermals: Their sedimentary expression on the New Zealand continental margin and in the deep sea. *Geology* 35(8):699–702.
38. DeConto RM, et al. (2012) Past extreme warming events linked to massive carbon release from thawing permafrost. *Nature* 484(7392):87–91.
39. Shellito LJ, Sloan LC, Huber M (2003) Evaluating pCO_2 levels in the early-middle Paleogene. *Palaeogeogr Palaeoclimatol Palaeoecol* 193:112–123.
40. Valdes P (2011) Built for stability. *Nat Geosci* 4:414–416.
41. Caballero R, Langen PL (2005) The dynamic range of poleward energy transport in an atmospheric general circulation model. *Geophys Res Lett* 32:L02705.
42. Lunt DJ, et al. (2012) A model–data comparison for a multi-model ensemble of early Eocene atmosphere–ocean simulations: EoMIP. *Climate of the Past* 8:1717–1736.
43. Abbot DS, Huber M, Bousquet G, Walker CC (2009) High-CO_2 cloud radiative forcing feedback over both land and ocean in a global climate model. *Geophys Res Lett* 36:L05702.
44. Goldner A, Huber M, Caballero R (2013) Does Antarctic glaciation cool the world? *Climate of the Past* 9:173–189.
45. Kump LR, Pollard D (2008) Amplification of Cretaceous warmth by biological cloud feedbacks. *Science* 320(5873):195.
46. Gregory JM, et al. (2004) A new method for diagnosing radiative forcing and climate sensitivity. *Geophys Res Lett* 31:L03205.
47. Colman R, Fraser J, Rotstayn L (2001) Climate feedbacks in a general circulation model incorporating prognostic clouds. *Climate Dynamics* 18(1-2):103–122.
48. Hansen J, et al. (2005) Efficacy of climate forcings. *J Geophys Res* 110:D18104.
49. Colman R, McAvaney B (2009) Climate feedbacks under a very broad range of forcing. *Geophys Res Lett* 36:L01702.
50. Goldblatt C, Lendon TM, Watson AJ (2009) An evaluation of the long-wave radiative transfer code used in the Met Office Unified Model. *Quarterly Journal of the Royal Meteorological Society* 135:619–633.
51. Andrews T, et al. (2012) Cloud adjustment and its role in CO_2 radiative forcing and climate sensitivity: A review. *Surveys in Geophysics* 33:619–635.
52. Caballero R, Huber M (2010) Spontaneous transition to superrotation in warm climates simulated by CAM3. *Geophys Res Lett* 37:L11701.
53. Arnold NP, Kuang Z, Tziperman E (2013) Enhanced MJO-like variability at high SST. *J Clim* 26(3):988–1001.
54. Bender FAM, Ramanathan V, Tselioudis G (2012) Changes in extratropical storm track cloudiness 1983–2008: Observational support for a poleward shift. *Climate Dynamics* 38(9-10):2037–2053.
55. Beven K (2006) A manifesto for the equifinality thesis. *Journal of Hydrology* 320: 18–36.
56. Bonham SG, Haywood AM, Lunt DJ, Collins M, Salzmann U (2009) El Niño-Southern Oscillation, Pliocene climate and equifinality. *Philos Trans A Math Phys Eng Sci* 367(1886):127–156.
57. Edwards TL, Crucifix M, Harrison SP (2007) Using the past to constrain the future: How the palaeorecord can improve estimates of global warming. *Progress in Physical Geography* 31:481–500.
58. Collins W, et al. (2006) The formulation and atmospheric simulation of the Community Atmosphere Model version 3 (CAM3). *J Clim* 19(11):2144–2161.
59. Yeager SG, Shields CA, Large WG, Hack JJ (2006) The low-resolution CCSM3. *J Clim* 19(11):2545–2566.
60. Sewall JO, et al. (2000) Climate sensitivity to changes in land surface characteristics. *Global Planet Change* 26(4):445–465.
61. Liu Z, et al. (2009) Global cooling during the eocene-oligocene climate transition. *Science* 323(5918):1187–1190.